# 3D Spectrum Sharing for Hybrid D2D and UAV Networks

Bodong Shang, Student Member, IEEE, Lingjia Liu, Senior Member, IEEE, Raghunandan M. Rao, Student Member, IEEE, Vuk Marojevic, Senior Member, IEEE, Jeffrey H. Reed, Fellow, IEEE

Abstract—In this paper, we study a three-dimensional (3D) spectrum sharing between device-to-device (D2D) and unmanned aerial vehicles (UAVs) communications. We consider that UAVs perform spatial spectrum sensing to opportunistically access the licensed channels that are occupied by the D2D communications of ground users. The objective of the considered 3D spectrum sharing networks is to maximize the area spectral efficiency (ASE) of UAV networks while guaranteeing the required minimum ASE of D2D networks. Using the tools from machine learning, we obtain the probability of spatial false alarm and the probability of spatial missed detection at the UAV, which helps us to characterize the density of active UAVs. Then, based on the Neyman-Pearson criterion, we further derive the coverage probability of D2D and UAV communications by leveraging the tools from stochastic geometry. In addition, the ASE of the D2D and UAV networks are also obtained. Simulation results show that a decrease in the spatial spectrum sensing radius of UAVs reduces the coverage probability of UAV communications but improves the ASE of UAV networks. Furthermore, the proposed tools allow obtaining the optimal spatial spectrum sensing radius of UAVs given certain network parameters.

*Index Terms*—UAV, D2D communications, spectrum sharing, heterogeneous networks, cognitive radio networks.

#### I. INTRODUCTION

NMANNED aerial vehicles (UAVs) have attracted great attention as they enable various applications and services [1]. Cellular operators consider UAVs as users or network support nodes in cellular networks and vehicle-to-everything communications [2]. In addition to operator deployed UAVs, UAVs may belong to third-party organizations or individuals who want to enjoy broadband data transmissions for video streaming, content delivery, surveillance report, etc. In the meantime, wireless communication systems for UAV data transmission need to be carefully designed. Due to the congested unlicensed spectrum, it is desirable for UAVs to transmit in licensed or shared spectrum [3]. Licensing spectrum for massive/broadband UAV communications is not

Manuscript received September 18, 2019; revised February 1, 2020; revised April 1, 2020; accepted May 14, 2020. Date of publication May xx, 2020; date of current version xxxx xx, 2020. The work of B. Shang and L. Liu is partially supported by US National Science Foundation (NSF) under grant CNS-1811720. The associate editor coordinating the review of this paper and approving it for publication was E. Basar. (*The corresponding author is L. Liu.*)

B. Shang, L, Liu, R. M. Rao and J. H. Reed are with Wireless@VT, The Bradley Department of ECE, Virginia Tech, VA, 24061, USA.

V. Marojevic is with Department of ECE, Mississippi State University, MS 39762, USA.

Digital Object Identifier xx.xxxx/TCOMM.2020.xxxxxxx

feasible; rather, we consider spectrum sharing between UAVs and ground licensed users to be a viable option.

In the licensed band, device-to-device (D2D) communications enable mobile users that are close to each other to communicate directly [4], [5]. The D2D operation in the licensed band includes the underlay mode (using the same spectrum as cellular communications links) and the overlay mode (using orthogonal spectrum to cellular communications) [6], [7]. D2D communications in the unlicensed band, on the other hand, need to coexist with WiFi networks and typically suffer severe interference [8]. Since D2D transceivers are in proximity of one another, the received interference power at D2D receivers (D2D-Rxs) from UAVs is lower, compared to that of the long range regime which occurs when the receiver lies outside the protection zone of D2D transmitters (D2D-Txs). Therefore, we consider the three dimensional (3D) spatial spectrum sharing between UAV and D2D communications where UAVs play the role of secondary users and D2D as primary users. To fully utilize the licensed spectrum in such hybrid D2D and UAV networks, we aim to maximize the area spectral efficiency (ASE) of UAV networks while guaranteeing the minimum required ASE for D2D users. From operators' perspective, sharing the licensed spectrum with UAVs can help them increase profit margins by charging fees from UAV users. From the UAVs' perspective, communications can achieve the desired performance in the licensed band, as opposed to the congested and insecure unlicensed band. Considering that mobile users need to pay monthly fees to the operator, D2D transmitters (D2D-Txs) are considered the primary and UAVs as the secondary users in the hybrid D2D-UAV spectrum sharing network. Since it is intractable to numerically calculate the conditional interference distributions (conditioned on the presence of D2D-Rx in the intersection of UAV sensing sphere and ground) at a UAV under the ground-to-air (G2A) channel models, we leverage machine learning tools, i.e., Gaussian kernel nonlinear regression, to approximately obtain the conditional interference distributions, which are used in the derivation of spatial false alarm and missed detection probabilities in UAV spatial spectrum sensing. Leveraging tools from stochastic geometry, we analytically derive the coverage probability of D2D communications and UAV communications. Based on our proposed model, we can maximize the area spectral efficiency (ASE) of UAV networks by optimizing the UAV spatial spectrum sensing radius under the constraint of a minimum ASE of D2D networks.

#### A. Related Works

Spectrum sharing in terrestrial networks has been investigated in [9]–[15]. In [9], the authors studied spectrum sharing for D2D communications in cellular networks. A paradigm for spectrum sharing between cellular communications and radio astronomy systems was introduced in [10]. In [11], the approach of guard zones (protection regions) around cellular BSs was introduced. The spatial spectrum sensing-based D2D communications have been studied in [12], [14] and have been extended to the D2D spectrum access in user-centric deployed heterogeneous networks [15].

On the other hand, 3D spectrum sharing for UAV networks has largely been unexplored. In [16], the authors derived the optimal density of spectrum sharing drone networks to maximize the throughput of the small cell UAV network. However, the considered channel model is rather simplistic to facilitate closed-form derivations. In [17], a spectrum sharing planning problem for a full-duplex UAV and underlaid D2D communications was studied, where a mobile UAV assists the communications between separated nodes without a direct link. In [18], the performance of a static UAV and a mobile UAV coexisting with D2D users in a finite area was studied, where the UAVs and D2D communications have the same spectrum access priority. [19], [20] also studied the coexistence of D2D and UAV communications. However, these works considered only one UAV in the sky in the absence of mutual interference between multiple UAVs with various flight heights. To the best of our knowledge, this is the first work that studies overlay spectrum sharing between UAVs and D2D communications from a system-level perspective.

#### B. Paper Contributions

The main contributions of our work are the following:

- 3D UAV Spatial Spectrum Sensing Model: A 3D UAV spatial spectrum sensing model for coexisting D2D and UAV networks is designed. The spatial spectrum sensing is conditioned on the sensing of D2D-Txs lying in the UAV's spatial spectrum sensing sphere. The conditional distributions of the received signal strength at the UAV have been approximated by log-normal distributions. Given network parameters, a machine learning-assisted approach is introduced to obtain the approximated distribution parameters (mean and standard deviation) to interpret the G2A channels. The spatial false alarm probability and the spatial missed detection probability of a typical UAV is obtained using the approximated conditional distributions.
- Coverage Probability and ASE Analysis: We model and analyze the 3D hybrid spectrum sharing network from a system-level perspective. Our model is flexible enough to capture any density distributions of UAVs in 3D space, rather than fixing the heights of UAVs. The coverage probability of D2D and UAV communications are derived by considering co-tier and cross-tier interference. Based

- on these analyses, we obtain the ASE of the D2D and UAV communications, respectively.
- Network Design Insights: The analysis and simulation results provide important network design insights: The optimal spatial spectrum sensing radius of UAVs is obtained to maximize the ASE of UAV networks under the constraint of a minimum ASE of D2D networks. It is observed that a decrease in the spatial spectrum sensing radius of UAVs has a contrasting effect on the coverage probability of UAV communications and the ASE of UAV networks. The optimal transmit power of UAVs can be also obtained which maximizes the ASE of UAV networks under the constraint of a minimum ASE of D2D networks.

The paper is organized as follows. Section II presents the system model. Section III gives the probabilities of spatial detection of a typical UAV. Section IV shows the coverage probabilities of D2D and UAV communications, and presents the ASE of UAV and D2D networks, respectively. Simulation and numerical results are discussed in Section V. Section VI concludes the paper.

#### II. SYSTEM MODEL

#### A. Network Layout

The network architecture is shown in Fig. 1. The locations of D2D transmitters (D2D-Txs) are modeled as a homogeneous Poisson point process (PPP) on the two dimensional (2D) ground with the density of  $\lambda_D$  and the set of D2D-Txs are denoted as  $\Phi_D$ . The signal-to-interference-plus-noise ratio (SINR) threshold of a D2D receiver (D2D-Rx) is  $\gamma_D^{th}$ . The transmit power of a D2D-Tx is  $P_D$ . Without loss of generality, we assume that UAVs are distributed in 3D space within the height range of  $[H_{\min}, H_{\max}]$ , where the densities of UAVs on different horizontal planes follow a certain distribution  $f_H(h)$ . Due to their flexible mobility, UAVs can fly at different heights and change their heights dynamically. Our model realistically captures the various heights of UAVs, unlike the state-of-the-art that assumes UAVs at a fixed height. We denote the 3D allowable flight space for UAVs as  $\mathbb{V}_A = \{(x, y, z) | H_{\min} \leq z \leq H_{\max} \}$ . The density of UAVs in  $V_A$  is  $\lambda_V$  which is the density of the ground projection points of UAVs. The set of all UAVs is represented by  $\Phi_V$ . In this paper, we consider the case where UAVs intend to transmit data to ground users in a same channel that is used by the overlaid D2D communications network. The transmit power of a UAV is denoted by  $P_V$  and the SINR threshold of the associated ground receiver is  $\gamma_V^{th}$ . The transmit power of UAV can be adapted according to the channel conditions and the user's quality of service requirement to further enhance the communication performance. Our model is applicable for many power control mechanisms such as the semi-static power control mechanism [21]. For ease of analysis, in this paper we assume fixed transmit power at UAVs.

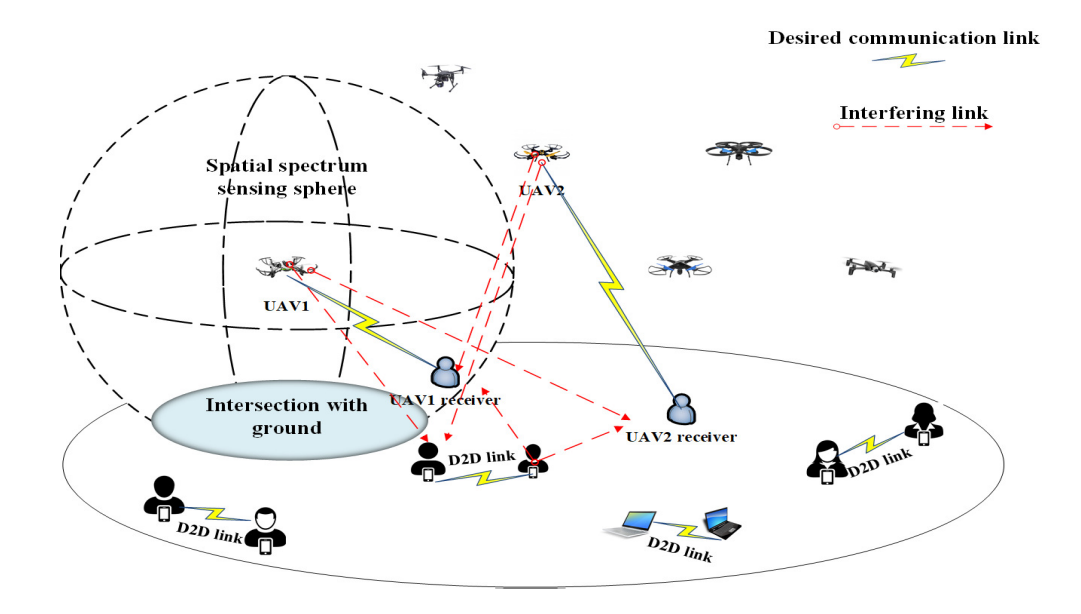


Fig 1: Spectrum sharing for D2D and UAV coexisting networks.

# B. Radio Propagation Model

The SINR of a typical D2D-Rx  $u_k^d$  associated with the corresponding D2D-Tx  $d_k$  is given by

$$SINR\left(u_{k}^{d}\right) = \frac{P_{D}h_{d_{k}u_{k}^{d}} \left\|d_{k} - u_{k}^{d}\right\|^{-\alpha_{GG}}}{I_{u_{k}^{d}}^{V} + I_{u_{k}^{d}}^{D} + \sigma_{n}^{2}}$$
where  $I_{u_{k}^{d}}^{V} = \sum_{v_{j} \in \Phi_{V}^{act}} \frac{P_{LOS}\left(v_{j}, u_{k}^{d}\right) P_{V} g_{v_{j}u_{k}^{d}}}{\left\|v_{j} - u_{k}^{d}\right\|^{\alpha_{AG}}}$ 

$$+ \sum_{v_{j} \in \Phi_{V}^{act}} \frac{P_{NLOS}\left(v_{j}, u_{k}^{d}\right) \eta P_{V} g_{v_{j}u_{k}^{d}}}{\left\|v_{j} - u_{k}^{d}\right\|^{\alpha_{AG}}}$$

$$I_{u_{k}^{d}}^{D} = \sum_{d_{j} \in \Phi_{D}, d_{j} \neq d_{k}} P_{D}h_{d_{j}u_{k}^{d}} \left\|d_{j} - u_{k}^{d}\right\|^{-\alpha_{GG}},$$

$$(1)$$

where  $h_{xy}$  denotes the channel power gain between ground nodes x and y which follows the Rayleigh distribution, ||a-b|| the distance between a and b, and  $\alpha_{GG}$  the path loss exponent from a ground node to another ground node.  $I_{u_k^d}^V$  is the aggregate interference power at  $u_k^d$  from active UÂVs,  $I_{u_k^d}^D$  is the aggregate interference power at  $u_k^d$  from D2D-Txs,  $\sigma_n^2$  is the noise power, and  $\Phi_V^{act}$  denotes the set of active UAVs which successfully access the channel through spatial spectrum sensing. For a ground D2D-Rx, the received interfering signals from active UAVs include LOS signals, Non-LOS (NLOS) signals, and multiple reflected components which cause multipath fading [22], [23].  $P_{LOS}(v_j, u_k^d)$  and  $P_{NLOS}\left(v_{j},u_{k}^{d}\right)$  denote the occurrence probabilities of the LOS and NLOS links between the  $j^{th}$  UAV  $v_j$  and the typical D2D-Rx  $u_k^d$ , where the summation of these two occurrence probabilities equals to one. Parameter  $\alpha_{AG}$  is the path loss exponent of the A2G link. The path loss is higher in a NLOS than in a LOS connection because of shadowing and indirect signal paths. Parameter  $\eta < 1$  is the excessive attenuation factor for NLOS. The Nakagami distribution can be used to describe the small scale fading in A2G and G2A channels [24], [25]. We use  $g_{xy}$  to denote the channel power gain between x and y in A2G and G2A connections which follows a normalized gamma distribution with parameter M.

Specifically, according to [23], we have

$$P_{LOS}\left(v_{j}, u_{k}^{d}\right) = \frac{1}{1 + C \exp\left[-B\left(\theta - C\right)\right]},$$
where  $\theta = \frac{180}{\pi} \arctan\left(\frac{h_{v_{j}}}{r_{v_{j}u_{k}^{d}}}\right),$ 
(2)

where C and B are constant values depending on the communications environment, e.g. rural, urban, or dense urban,  $h_{v_j}$  is the height of the UAV  $v_j$ , and  $r_{v_ju_k^d}$  denotes the horizontal distance between UAV  $v_j$  and D2D-Rx  $u_k^d$ . In addition, we have  $P_{NLOS}\left(v_j,u_k^d\right)=1-P_{LOS}\left(v_j,u_k^d\right)$ .

The SINR of a typical UAV receiver (UAV-Rx)  $u_i^v$  associated with UAV  $v_i$  is given by

$$SINR\left(u_{i}^{v}\right) = \frac{P_{V}L\left(v_{i}, u_{i}^{v}\right)g_{v_{i}u_{i}^{v}}\left\|v_{i} - u_{i}^{v}\right\|^{-\alpha_{AG}}}{I_{u_{i}^{v}}^{V} + I_{u_{i}^{v}}^{D} + \sigma_{n}^{2}}$$
where
$$L\left(v_{i}, u_{i}^{v}\right) = P_{LOS}\left(v_{i}, u_{i}^{v}\right) + \eta P_{NLOS}\left(v_{i}, u_{i}^{v}\right),$$

$$I_{u_{i}^{v}}^{D} = \sum_{d_{j} \in \Phi_{D}} P_{D}h_{d_{j}u_{i}^{v}}\left\|d_{j} - u_{i}^{v}\right\|^{-\alpha_{GG}}$$

$$I_{u_{i}^{v}}^{V} = \sum_{v_{j} \in \Phi_{V}^{act}, v_{j} \neq v_{i}} \frac{P_{LOS}\left(v_{j}, u_{i}^{v}\right)P_{V}g_{v_{j}u_{i}^{v}}}{\left\|v_{j} - u_{i}^{v}\right\|^{\alpha_{AG}}}$$

$$+ \sum_{v_{j} \in \Phi_{V}^{act}, v_{j} \neq v_{i}} \frac{P_{NLOS}\left(v_{j}, u_{i}^{v}\right)\eta P_{V}g_{v_{j}u_{i}^{v}}}{\left\|v_{j} - u_{i}^{v}\right\|^{\alpha_{AG}}},$$

$$(3)$$

where  $P_{LOS}\left(v_{i},u_{i}^{v}\right)$  and  $P_{NLOS}\left(v_{i},u_{i}^{v}\right)$  are the occurrence probabilities of LOS and NLOS connections between the typical UAV  $v_{i}$  and its associated receiver  $u_{i}^{v}$ . The term  $I_{u_{i}^{v}}^{V}$  in

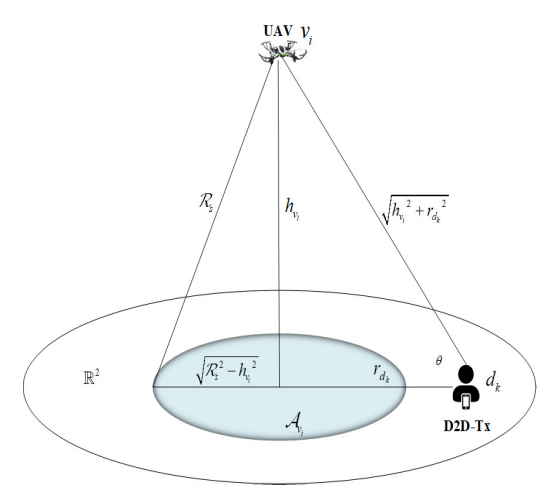


Fig 2: Ground intersection of spectrum sensing region of a typical UAV.

(3) represents the aggregate interference power at the typical ground UAV-Rx  $u_i^v$  caused by the active UAVs .  $I_{u_i^v}^D$  is the aggregate interference power at  $u_i^v$  caused by the D2D-Txs.

# C. Spatial Spectrum Sensing

We define the spatial spectrum sensing sphere of a typical UAV  $v_i$  at the height of  $h_{v_i}$  as

$$\mathcal{S}_{v_i} = \left\{ v\left(x_v, y_v, z_v\right) \in \mathbb{V}^3 \middle| \|v_i - v\| \leqslant \mathcal{R}_s \right\}$$

$$||v_i - v|| = \sqrt{(x_{v_i} - x_v)^2 + (y_{v_i} - y_v)^2 + (h_{v_i} - z_v)^2},$$
(4)

where  $x_v$ ,  $y_v$  and  $z_v$  represent the coordinates of the point v,  $\mathbb{V}^3$  denotes the 3D space,  $\|v_i-v\|$  is the spatial distance between UAV  $v_i$  and  $v\left(x_v,y_v,z_v\right)$ , and  $\mathcal{R}_s$  is the spatial spectrum sensing radius of UAV. The intersection between  $\mathcal{S}_{v_i}$  and the ground is denoted by  $\mathcal{A}_{v_i} = \mathcal{S}_{v_i} \cap \mathbb{R}^2$ , where  $\mathbb{R}^2$  is the horizontal ground plane. More specifically, we have

$$A_{v_i} = \left\{ m(x_m, y_m) \in \mathbb{R}^2 | \|v_i - m\| \leqslant \sqrt{{R_s}^2 - {h_{v_i}}^2} \right\}$$

and

$$||v_i - m|| = \sqrt{(x_{v_i} - x_m)^2 + (y_{v_i} - y_m)^2},$$
 (5)

where  $m(x_m, y_m)$  denotes a point located in  $\mathcal{A}_{v_i}$ , and  $(x_m, y_m)$  are its coordinates. Expression  $||v_i - m||$  is the horizontal distance between UAV  $v_i$  and ground point m. Fig. 2 illustrates the geometrical setup and parameters.

Let  $\mathcal{H}^0$  be the event that there is no D2D-Tx in  $\mathcal{A}_{v_i}$ , and  $\mathcal{H}^1$  be the event that there is at least one D2D-Tx in  $\mathcal{A}_{v_i}$ . We assume that in each time slot of duration T, all UAVs first perform spatial spectrum sensing of duration  $\tau$ , and the UAVs which access the channel transmit data in the remaining time duration  $T - \tau$ . At UAV  $v_i$ , the received signals y[n] during spatial spectrum sensing for the events  $\mathcal{H}^0$  and  $\mathcal{H}^1$  are given in (6) and (7), where n is the sample index,  $s_{d_k}[n]$  is the  $n^{th}$  sample from D2D-Tx  $d_k$ , and the noise  $n_0[n]$  is i.i.d.

circularly symmetric complex Gaussian with zero mean and variance  $\sigma_n^2$ :

$$\mathcal{H}^{0}: y [n] = \sum_{d_{k} \in \Phi_{D}, d_{k} \notin \mathcal{A}_{v_{i}}} P_{LOS}(d_{k}, v_{i}) \sqrt{\frac{P_{D}g_{d_{k}v_{i}}}{\|d_{k} - v_{i}\|^{\alpha_{GA}}}} s_{d_{k}} [n]$$

$$+ \sum_{d_{k} \in \Phi_{D}, d_{k} \notin \mathcal{A}_{v_{i}}} P_{NLOS}(d_{k}, v_{i}) \sqrt{\frac{P_{D}\eta g_{d_{k}v_{i}}}{\|d_{k} - v_{i}\|^{\alpha_{GA}}}} s_{d_{k}} [n]$$

$$+ n_{0} [n],$$

$$\mathcal{H}^{1}: y [n]$$

$$= \sum_{d_{k} \in \Phi_{D}, \Phi_{D} \cap \mathcal{A}_{v_{i}} \neq \emptyset} P_{LOS}(d_{k}, v_{i}) \sqrt{\frac{P_{D}g_{d_{k}v_{i}}}{\|d_{k} - v_{i}\|^{\alpha_{GA}}}} s_{d_{k}} [n]$$

$$+ \sum_{d_{k} \in \Phi_{D}, \Phi_{D} \cap \mathcal{A}_{v_{i}} \neq \emptyset} P_{NLOS}(d_{k}, v_{i}) \sqrt{\frac{P_{D}\eta g_{d_{k}v_{i}}}{\|d_{k} - v_{i}\|^{\alpha_{GA}}}} s_{d_{k}} [n]$$

$$+ n_{0} [n].$$

$$(7)$$

The test statistics of the received signals at a typical UAV are given by

$$\Gamma | I^{\varpi} = \frac{1}{N_s} \sum_{n=0}^{N_s - 1} |y[n]|^2, \quad \varpi = \{0, 1\},$$
 (8)

where  $N_s$  denotes the number of samples. When  $N_s$  is large, the distribution approaches a conditional Gaussian distribution because of the central limit theorem, i.e.,

$$\Gamma | I^{\varpi} \sim \mathcal{N} \left( I^{\varpi} + \sigma_n^2, \frac{\left( I^{\varpi} + \sigma_n^2 \right)^2}{N_s} \right).$$
 (9)

The mean and the variance of the conditional Gaussian distribution depend on the hypothesis [26], [14]. Note that  $I^0$  and  $I^1$  are random variables that depend on the network topology, D2D-Tx density and transmit powers, channel conditions, height of the sensing-based UAV and its spatial spectrum sensing radius.  $I^0$  and  $I^1$  are expressed as

$$I^{0} = \sum_{d_{k} \in \Phi_{D}, d_{k} \notin \mathcal{A}_{v_{i}}} P_{LOS}(d_{k}, v_{i}) \frac{P_{D}g_{d_{k}v_{i}}}{\|d_{k} - v_{i}\|^{\alpha_{GA}}} + \sum_{d_{k} \in \Phi_{D}, d_{k} \notin \mathcal{A}_{v_{i}}} P_{NLOS}(d_{k}, v_{i}) \frac{P_{D}\eta g_{d_{k}v_{i}}}{\|d_{k} - v_{i}\|^{\alpha_{GA}}},$$

$$(10)$$

$$I^{1} = \sum_{d_{k} \in \Phi_{D}, \Phi_{D} \cap \mathcal{A}_{v_{i}} \neq \emptyset} P_{LOS}\left(d_{k}, v_{i}\right) \frac{P_{D}g_{d_{k}v_{i}}}{\left\|d_{k} - v_{i}\right\|^{\alpha_{GA}}} + \sum_{d_{k} \in \Phi_{D}, \Phi_{D} \cap \mathcal{A}_{v_{i}} \neq \emptyset} P_{NLOS}\left(d_{k}, v_{i}\right) \frac{P_{D}\eta g_{d_{k}v_{i}}}{\left\|d_{k} - v_{i}\right\|^{\alpha_{GA}}}.$$

$$(11)$$

The spatial false alarm probability and the spatial missed detection probability of a UAV are

$$P_{fa} = \mathbb{E}_{I^0} \left\{ \mathbb{P} \left( \Gamma > \varepsilon | \mathcal{H}^0 \right) \right\}, \tag{12}$$

$$P_{md} = \mathbb{E}_{I^1} \left\{ \mathbb{P} \left( \Gamma < \varepsilon | \mathcal{H}^1 \right) \right\}, \tag{13}$$

where  $\varepsilon$  is the energy detection threshold. The essential differ-

ence of spectrum sharing between 3D and 2D networks is the unknown conditional distribution of the aggregated received power at the UAV which determines the false alarm and missed detection probabilities.

If the test statistics received power  $\Gamma$  at a UAV is greater than  $\varepsilon$ , the UAV will transmit with probability  $\beta_1$ , otherwise, it will transmit with probability  $\beta_0$ , where  $\beta_0 > \beta_1$ . Therefore, for event  $\mathcal{H}^0$ , a UAV will access the licensed channel with probability

$$P^{0} = P_{fa}\beta_{1} + (1 - P_{fa})\beta_{0}. \tag{14}$$

For event  $\mathcal{H}^1$ , a UAV will access the licensed channel with probability

$$P^{1} = (1 - P_{md}) \beta_{1} + P_{md} \beta_{0}.$$
 (15)

Note that  $P_{fa}$  and  $P_{md}$  are key performance metrics for the UAVs spatial spectrum sensing, affecting the density of active UAVs and the co-channel interference to UAV and D2D communications. This will provide useful insights to design efficient spectrum sharing strategies that balance the aggressive spectrum reuse and the resulting co-channel interference. Compared with the modeling and analysis in conventional heterogeneous networks [27], the technical challenges of analyzing spectral sharing opportunities between UAV and D2D networks include modeling the height dependent spectrum access, determining the distributions of the aggregated received power during spectrum sensing, and characterizing network interference in 3D.

# III. FALSE ALARM PROBABILITY AND MISSED DETECTION PROBABILITY ANALYSIS

In this section, we provide the intermediate technical results for the system-level performance analysis, where we characterize the probability of spatial false alarm and the probability of spatial missed detection of a typical UAV. These probabilities will be used to determine the density of active UAVs and the interference from active UAVs.

# A. Probability of Spatial False Alarm

For a typical UAV  $v_i$  at the height of  $h_{v_i}$ , since  $I^0$  in (10) is a random variable relying on the network parameters, the probability of spatial false alarm  $P_{fa}$  in (12) can be expressed as

$$P_{fa} = \int_0^\infty \mathbb{P}\left(\Gamma > \varepsilon | \mathcal{H}^0, I^0 = x\right) f_{I^0}(x) dx, \qquad (16)$$

where  $f_{I^0}(x)$  is the probability density function (PDF) of  $I^0$ .

We derive the Laplace transform of  $I^0$  when  $\mathcal{R}_s > h_{v_i}$  to determine its distribution which is shown in (17), where (a) is obtained from the expectation of the normalized gamma distribution. In addition, when  $\mathcal{R}_s \leq h_{v_i}$ , we have

$$\mathcal{L}_{I^{0}|\mathcal{R}_{s} \leqslant h_{v_{i}}}(s)$$

$$= \exp\left\{-2\pi\lambda_{D}\right.$$

$$\cdot \int_{0}^{\infty} \left[1 - \left(1 + \xi\left(x, P_{D}\right) + \Theta\left(x, P_{D}\right)\right)^{-M}\right] x dx\right\}.$$
(18)

Using the Probability Density Function (PDF) of  $I^0$ , i.e.,  $f_{I^0|.}(t)$ , the Laplace transform of  $I^0$  is expressed as

$$\mathcal{L}_{I^{0}|\cdot}(s) = \mathbb{E}\left\{e^{-sI_{0}}\right\} = \int_{0}^{\infty} e^{-st} f_{I^{0}|\cdot}(t)dt,$$
(19)

where  $I^0 \mid$  denotes the event  $I^0$  under  $\mathcal{R}_s > h_{v_i}$  or  $\mathcal{R}_s \leqslant h_{v_i}$ . The PDF can then be derived by taking the inverse Laplace transform:

$$f_{I^{0}|\cdot}(t) = \mathcal{L}^{-1} \left\{ \mathcal{L}_{I^{0}|\cdot}(s) \right\}$$

$$= \frac{1}{2\pi i} \lim_{T \to \infty} \int_{\gamma = iT}^{\gamma + iT} e^{st} \mathcal{L}_{I^{0}|\cdot}(s) ds.$$
(20)

Note that there are several other methods for deriving the distributions of  $I_0$  and  $I_1$  such as the inverse transform of characteristic function. However, these analytical methods involve multiple integrals and integrals in a complex domain which impede tractable algorithm design.

The probability of spatial false alarm can be calculated by combining (20) into (16) as follows:

$$P_{fa} = \begin{cases} \int_0^\infty \zeta(x) f_{I^0|\mathcal{R}_s > h_{v_i}}(x) dx, & \mathcal{R}_s > h_{v_i} \\ \int_0^\infty \zeta(x) f_{I^0|\mathcal{R}_s \leq h_{v_i}}(x) dx, & \mathcal{R}_s \leq h_{v_i} \end{cases}, (21)$$

where 
$$\zeta\left(x\right)=Q\left(\frac{\varepsilon-x-{\sigma_n}^2}{x+{\sigma_n}^2}\sqrt{N}\right)$$
 and  $Q\left(\cdot\right)$  is the Q-function.

# B. Probability of Spatial Missed Detection

Similar to the derivation of  $P_{fa}$ , the Laplace transform of  $I^1$  when  $\mathcal{R}_s > h_{v_i}$  is obtained in (22), where  $\xi(x)$  and  $\Theta(x)$  are given in (17).

Therefore, the probability of spatial missed detection can be expressed as

$$P_{md} = \begin{cases} \int_0^\infty (1 - \zeta(x)) f_{I^1 \mid \mathcal{R}_s > h_{v_i}}(x) dx, \mathcal{R}_s > h_{v_i} \\ 0, \mathcal{R}_s \leqslant h_{v_i} \end{cases}$$
(23)

Remark 1. In terrestrial communications with 2D Poisson distributed interfering nodes, the closed form PDF of  $I^0$  can be approximated by the inverse Gaussian distribution [28] and the log-normal distribution [29] by taking the first, second and/or third order cumulants. However, these approximations do not match well with the exact values of  $I^0$  and  $I^1$  in 3D networks. Therefore, it is crucial to obtain the simple and tractable approximated distributions of the aggregate interference for 3D UAV spectrum sensing to provide useful system design guidelines.

# C. Machine Learning-Assisted Approach

It is difficult to compute  $P_{fa}$  and  $P_{md}$  numerically in (21) and (23) due to multiple integrals in the calculation of the inverse Laplace transform. The nonlinear regression technique can be used to obtain the approximated PDFs of  $I^0$  and  $I^1$  to facilitate system-level performance analysis [30]. Due to the exponential distance dependent large-scale path-loss, the PDFs of the aggregated received signal strength  $I^0$  and  $I^1$  at a UAV are concentrated within certain values and have a

$$\mathcal{L}_{I^{0}|\mathcal{R}_{s}>h_{v_{i}}}(s) \\
= \mathbb{E}\left\{\exp\left(-sI^{0}|\mathcal{R}_{s}>h_{v_{i}}\right)\right\} \\
= \mathbb{E}_{\Phi_{D}}\left\{\prod_{d_{k}\in\Phi_{D},d_{k}\notin\mathcal{A}_{v_{i}}}\mathbb{E}_{g}\left\{\exp\left(-s\frac{P_{LOS}(d_{k},v_{i})P_{D}g_{d_{k}v_{i}}}{\|d_{k}-v_{i}\|^{\alpha GA}} - s\frac{P_{NLOS}(d_{k},v_{i})P_{D}\eta g_{d_{k}v_{i}}}{\|d_{k}-v_{i}\|^{\alpha GA}}\right)\right\}\right\} \\
= \exp\left\{-2\pi\lambda_{D}\int_{\sqrt{\mathcal{R}_{s}^{2}-h_{v_{i}}^{2}}}^{\infty}\left[1 - (1+\xi(x,P_{D})+\Theta(x,P_{D}))^{-M}\right]xdx\right\} \\
\text{where } \xi(x,P_{D}) = \frac{\frac{sP_{D}}{M}(x^{2}+h_{v_{i}}^{2})^{-\frac{\alpha GA}{2}}}{1+C\exp\left[-B\left(E\arctan\left(\frac{h_{v_{i}}}{x}\right)-C\right)\right]},\Theta(x,P_{D}) = \frac{sP_{D}\eta\left(x^{2}+h_{v_{i}}^{2}\right)^{-\frac{\alpha GA}{2}}}{M} - \eta\xi(x,P_{D}), \\
\mathcal{L}_{I^{1}|\mathcal{R}_{s}>h_{v_{i}}}(s) \\
= \mathbb{E}\left\{\exp\left(-sI^{1}|\mathcal{R}_{s}>h_{v_{i}}\right)\right\} \\
= \mathbb{E}_{\Phi_{D}}\left\{\prod_{d_{k}\in\Phi_{D}\cap\mathcal{A}_{v_{i}}}^{\infty}\Phi_{D}\cap\mathcal{A}_{v_{i}}\neq\emptyset}\mathbb{E}_{g}\left\{\exp\left(-s\frac{P_{LOS}(d_{k},v_{i})P_{D}g_{d_{k}v_{i}} + P_{NLOS}(d_{k},v_{i})P_{D}\eta g_{d_{k}v_{i}}}{\|d_{k}-v_{i}\|^{\alpha GA}}\right)\right\}\right\} \\
\cdot \mathbb{E}_{\Phi_{D}}\left\{\prod_{d_{k}\in\Phi_{D}\cap\mathcal{A}_{v_{i}}^{\infty}}\mathbb{E}_{g}\left\{\exp\left(-s\frac{P_{LOS}(d_{k},v_{i})P_{D}g_{d_{k}v_{i}} + P_{NLOS}(d_{k},v_{i})P_{D}\eta g_{d_{k}v_{i}}}{\|d_{k}-v_{i}\|^{\alpha GA}}\right)\right\}\right\} \\
= \frac{e^{-2\pi\lambda_{D}\int_{0}^{\infty}\left[1-(1+\xi(x,P_{D})+\Theta(x,P_{D}))^{-M}\right]xdx}}{1-\exp\left[-\lambda_{D}\pi\left(\mathcal{R}_{s}^{2}-h_{v_{i}}^{2}\right)\right]}, \tag{22}$$

long tail. Without loss of generality, we make the following proposition.

**Proposition 1.** The PDFs of the received signal strength  $I^0$  and  $I^1$  for the events  $\mathcal{H}^0$  and  $\mathcal{H}^1$  can be well approximated by the log-normal distribution with appropriate mean and standard deviation values. More specifically, we have

$$f_{I^{\varpi}}(x) \approx \frac{1}{x\sigma_{I^{\varpi}}\sqrt{2\pi}} \exp\left[-\frac{\left(\ln x - \mu_{I^{\varpi}}\right)^2}{2\sigma_{I^{\varpi}}^2}\right],$$
 (24)

where  $\mu_{I^{\varpi}}$  and  $\sigma_{I^{\varpi}}$  are the mean and the standard deviation variables.

Note that other families of distributions such as the inverse gamma or scaled inverse chi-squared can be used to approximate the distributions. However, the choice of approximate distribution model is beyond the scope of this paper where we focus on the system-level performance evaluation.

In terrestrial communications with 2D Poisson distributed interfering nodes, the values of  $\mu_{I^0}$  and  $\sigma_{I^0}$  can be obtained by calculating the first and second cumulants of  $I^0$  [28]. However, the results obtained by the first and second cumulants of  $I^0$  are no longer accurate under 3D UAV channels due to the LOS and NLOS nature of G2A connections. The Gaussian kernel nonlinear regression is used to explore the relationship between input (network parameters) and output (mean and the standard deviation of log-normal distribution). In Fig. 3, the input network parameters are the density  $\lambda_D$  of D2D-Txs, UAV's flight height  $h_{v_i}$ , UAV's spatial spectrum sensing radius  $\mathcal{R}_s$ , and the channel power gain M of G2A transmission. The output is the mean or the standard deviation of the

approximated log-normal distribution of  $I^{\varpi}, \varpi = \{0, 1\}.$ 

**Remark 2.** In the training process, the transmit power of D2D-Txs is not set as an input. We use the scaling property of the log-normal distribution to update the mean value of the approximated log-normal distribution, i.e, if  $I^{\varpi} \sim \text{Lognormal}(\mu_{I^{\varpi}}, \sigma_{I^{\varpi}})$ , then we have  $aI^{\varpi} \sim \text{Lognormal}(\mu_{I^{\varpi}} + \ln a, \sigma_{I^{\varpi}})$ .

We use Monte Carlo simulations with diverse input values to generate the data set for training. For this data set generation, the mean and the standard deviation values of the log-normal distribution can be obtained as follows

$$\mu_{I^{\varpi}} = \ln \left( \frac{\mathbb{E}\{I^{\varpi}\}^{2}}{\sqrt{\mathbb{E}\left\{(I^{\varpi})^{2}\right\}}} \right), \tag{25}$$

$$\sigma_{I^{\varpi}} = \left[ \ln \left( \frac{\mathbb{E}\left\{ (I^{\varpi})^{2} \right\}}{\mathbb{E}\left\{ I^{\varpi} \right\}^{2}} \right) \right]^{\frac{1}{2}}.$$
 (26)

We denote the input variables as  $\mathbf{x}^{(i)} = \begin{bmatrix} x_1^{(i)}, x_2^{(i)}, x_3^{(i)}, x_4^{(i)} \end{bmatrix}$  (corresponding to the network parameters  $\lambda_D$ ,  $h_{v_i}$ ,  $\mathcal{R}_s$ , M). The output variable is denoted by  $y^{(i)}$  (corresponding to the  $\mu_{I^{\varpi}}$  or  $\sigma_{I^{\varpi}}$ ,  $\varpi = \{0,1\}$ ), where (i) indicates the data set index. To balance the weights of the different inputs, we normalize the input variables between 0 and 1 as follows

$$\widetilde{x}_j^{(i)} = \frac{x_j^{(i)} - \min\left(\mathbf{x}_j\right)}{\max\left(\mathbf{x}_j\right) - \min\left(\mathbf{x}_j\right)}, j = 1, \dots, 4,$$
 (27)

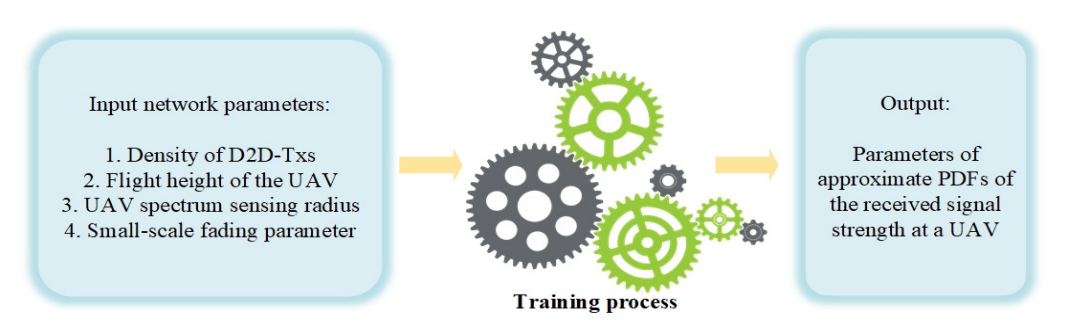


Fig 3: Input and output of the machine learning-based approach.

where  $\mathbf{x}_j = \left[x_j^{(1)}, \cdots, x_j^{(L)}\right]$  and L is the number of inputoutput pairs in the generated data set. We then obtain the normalized input variables  $\widetilde{\mathbf{x}}^{(i)} = \left[\widetilde{x}_1^{(i)}, \widetilde{x}_2^{(i)}, \widetilde{x}_3^{(i)}, \widetilde{x}_4^{(i)}\right]$ .

To estimate the output value given the input network parameters, we use the Gaussian Kernel function to calculate the weighted average output values as follows

$$f(x) = \frac{1}{\sqrt{2\pi\sigma_G^2}} \exp\left[-\frac{(x-\mu_G)^2}{2\sigma_G^2}\right],$$
 (28)

where  $\mu_G$  and  $\sigma_G$  are the mean and the standard deviation of the Gaussian kernel function.

The query point is denoted by  $\mathbf{q} = [q_1, q_2, q_3, q_4]$ , which collects the local information of the data set. The distance between the query point  $\mathbf{q}$  and the normalized data point  $\widetilde{\mathbf{x}}^{(i)}$ , i.e.,  $D(\mathbf{q}, \widetilde{\mathbf{x}}^{(i)})$ , is given by

$$D\left(\mathbf{q}, \widetilde{\mathbf{x}}^{(i)}\right) = \sqrt{\left(\mathbf{q} - \widetilde{\mathbf{x}}^{(i)}\right) \left(\mathbf{q} - \widetilde{\mathbf{x}}^{(i)}\right)^{\mathrm{T}}}.$$
 (29)

Note that the term  $\frac{1}{\sqrt{2\pi\sigma_G^2}}$  in (28) will not impact the weighted average value at the query point q. Therefore, the kernel function in the training process can be expressed as

$$K\left(\mathbf{q}, \widetilde{\mathbf{x}}^{(i)}\right) = \exp\left(-\frac{D\left(\mathbf{q}, \widetilde{\mathbf{x}}^{(i)}\right)^{2}}{2\sigma_{G}^{2}}\right),$$
 (30)

where  $D\left(\mathbf{q}, \widetilde{\mathbf{x}}^{(i)}\right)$  is given in (29). Then, the estimate output value at the query point  $\mathbf{q}$  is

$$\widehat{y}(\mathbf{q}) = \frac{\sum_{i=1}^{L} \left( K\left(\mathbf{q}, \widetilde{\mathbf{x}}^{(i)}\right) y^{(i)} \right)}{\sum_{i=1}^{L} K\left(\mathbf{q}, \widetilde{\mathbf{x}}^{(i)}\right)},$$
(31)

where  $K\left(\mathbf{q},\widetilde{\mathbf{x}}^{(i)}\right)$  represents the weight value of the inputoutput pair  $\left(\widetilde{\mathbf{x}}^{(i)},y^{(i)}\right)$ . After evaluating (31) over a range of query points, given an input combination of the network parameters, we can search the nearest query point to the inputs and obtain the corresponding output value. After that, we use the approximated PDFs of  $I^0$  and  $I^1$  in (21) and (23) to obtain the approximated spatial false alarm probability and spatial missed detection probability.

In detection theory, the Neyman-Pearson criterion says that one can minimize the spatial missed detection probability  $P_{md}$  while not allowing the spatial false alarm probability  $P_{fa}$  to exceed a predefined value  $P_{fa}^*$ , i.e.,  $P_{fa} \leq P_{fa}^*$ , or minimize

 $P_{fa}$  subject to a constraint on  $P_{md}$ . In this paper, we assume a constant  $P_{fa} = P_{fa}^*$ . Therefore, the spatial spectrum sensing radius and the energy detection threshold of a UAV are coupled through the UAV's spatial spectrum sensing. In practical engineering design, based on the policy  $P_{fa} = P_{fa}^*$ , we can adjust the energy detection threshold to change the spatial spectrum sensing radius. It is worth noting that the proposed machine learning-assisted approach is applicable to other user distributions such as Poisson cluster process and Poisson hole process. However, the exact closed-form analytical expression of energy detection threshold cannot be derived for these, which provides few information in performance optimization.

#### IV. SYSTEM-LEVEL PERFORMANCE ANALYSIS

In this section, we derive the coverage probability of a typical D2D communication network and the coverage probability of a typical UAV communication network conditioned on the UAV's flight height  $h_{v_i}$  and the distance  $r_i^v$  between UAV-Rx  $u_i^v$  and the projection of its associated UAV  $v_i$  on the ground. These results will be used to determine the ASE of the D2D and UAV networks.

Note that a UAV can access the licensed channel with probability  $P^0 = P_{fa}\beta_1 + (1-P_{fa})\beta_0$  for event  $\mathcal{H}^0$  and with probability  $P^1 = (1-P_{md})\beta_1 + P_{md}\beta_0$  for event  $\mathcal{H}^1$ , where  $P_{fa}$  and  $P_{md}$  are given in (21) and (23), respectively, and the PDFs of  $I^0$  and  $I^1$  are given in Proposition 1 with its parameters trained using a Gaussian nonlinear kernel-based machine learning method.

**Lemma 1.** In the spatial spectrum sensing process, the channel access probability  $P^0$  under event  $\mathcal{H}^0$  is greater than the channel access probability  $P^1$  under event  $\mathcal{H}^1$ .

*Proof.* Please refer to Appendix A for the proof. 
$$\Box$$

It's worth noting that UAVs at different heights experience different aggregated received powers from D2D transmissions because of the varying elevation angles and intersection region between the spatial spectrum sensing sphere and ground. The specific aggregated received power at each UAV leads to different secondary channel access probabilities. In other words, UAVs at different flight heights will generate different levels of interference to the primary D2D network on the ground. For analytical tractability, we uniformly divide the height  $\mathbb{V}_A$  into N sub-regions with a common thickness of  $\Delta H$ , i.e.,

$$H_{\text{max}} - H_{\text{min}} = N \cdot \Delta H. \tag{32}$$

$$\mathbb{P}_{D}^{c} | l_{k}^{d} = \exp\left(-\frac{2\pi^{2} \lambda_{D} \gamma_{D}^{th} \frac{2}{\alpha_{GG}} (l_{k}^{d})^{2}}{\alpha_{GG} \sin\left(\frac{2\pi}{\alpha_{GG}}\right)} - 2\pi \sum_{n=1}^{N_{h}} P_{UAV}^{act,n} \lambda_{V,H_{n}} \int_{\sqrt{\mathcal{R}_{s}^{2} - H_{n}^{2}}}^{\infty} x\Omega\left(x, H_{n}\right) dx\right) \\
\cdot \exp\left(-2\pi \sum_{n=N_{h}+1}^{N} P^{0} \lambda_{V,H_{n}} \int_{0}^{\infty} x\Omega\left(x, H_{n}\right) dx - \frac{\gamma_{D}^{th} \sigma_{n}^{2}}{P_{D} (l_{k}^{d})^{-\alpha_{GG}}}\right) \\
\text{where } P_{UAV}^{act,n} = P^{1} + (P^{0} - P^{1}) e^{-\pi \lambda_{D} (\mathcal{R}_{s}^{2} - H_{n}^{2})} \\
\Omega\left(x, H_{n}\right) = 1 - \left(1 + \Delta\left(x, H_{n}\right) \frac{\eta_{M} \gamma_{D}^{th} P_{V} \left(x^{2} + H_{n}^{2}\right)^{-\frac{\alpha_{AG}}{2}}}{M P_{D} (l_{k}^{d})^{-\alpha_{GG}}} + (1 - \Delta\left(x, H_{n}\right)) \frac{\eta_{M} \gamma_{D}^{th} P_{V} \eta\left(x^{2} + H_{n}^{2}\right)^{-\frac{\alpha_{AG}}{2}}}{M P_{D} (l_{k}^{d})^{-\alpha_{GG}}}\right)^{-M} \\
\Delta\left(x, H_{n}\right) = \frac{1}{1 + C \exp\left[-B\left(E \arctan\left(H_{n}/x\right) - C\right)\right]}, \eta_{M} = M(M!)^{-\frac{1}{M}},$$
(35)

 $H_n$  approximates the height of UAVs in the  $n^{th}$  sub-region  $\mathbb{V}(x,y,H_n)$ . In  $\mathbb{V}(x,y,H_n)$ , we assume that UAVs are uniformly distributed on the horizontal plane at height  $H_n$ . The set of UAVs in  $\mathbb{V}(x,y,H_n)$  is denoted as  $\Phi_{V,H_n}$ . Considering the randomness of UAV locations, we assume that  $\Phi_{V,H_n}$ follows a homogeneous PPP with density  $\lambda_{V,H_n}$ , where

$$\lambda_{V,H_n} = \lambda_V \int_{H_n}^{H_n + \Delta H} f_H(h) dh. \tag{33}$$

If  $\mathcal{R}_s > H_n$ , the active probability of UAVs in  $\Phi_{V,H_n}$  is statistically equivalent to the case where all UAVs in  $\Phi_{V,H_n}$ transmit with probability  $P^1$  and additionally the UAVs in  $\Phi_{V,H_n}$ , which have no D2D-Txs within their spatial spectrum sensing spheres, transmit with probability  $P^0 - P^1$ . Thus, the average channel access probability of UAVs at height  $H_n$  is

$$P_{UAV}^{act,n} = P^1 + (P^0 - P^1) e^{-\pi \lambda_D (\mathcal{R}_s^2 - H_n^2)}.$$
 (34)

For analytical tractability, we approximate the locations of active UAVs in  $\mathbb{V}(x, y, H_n)$  as randomly distributed with the density of  $P_{UAV}^{act,n} \lambda_{V,H_n}$ .  $\Phi_{V,H_n}^{L'}$  denotes the set of active UAVs in  $\mathbb{V}(x, y, H_n)$ .

If  $\mathcal{R}_s \leqslant H_n$ , all UAVs in  $\mathbb{V}(x,y,H_n)$  will transmit with probability  $P^0$ . Thus, the locations of active UAVs are modeled by a PPP  $\Phi^S_{V,H_n}$  with density  $P^0\lambda_{V,H_n}.$ 

We are now in the position of computing the coverage probability of a typical D2D communication network and a typical UAV communication network.

#### A. Coverage Probability of D2D Communications

We obtain the coverage probability of a typical D2D-Rx in the following theorem.

**Theorem 1.** The coverage probability of a typical D2D-Rx  $u_k^d$  conditioned on the D2D serving distance  $l_k^d$  is given in equation (35).

## B. Coverage Probability of UAV Communications

A typical ground UAV-Rx receives interference from D2D and UAV communications. Note that the desired serving link distance of a typical UAV  $v_i$  is dependent on UAV's flight height and distance  $r_i^v$  which is the distance between UAV-Rx and the projection of UAV on the ground.

**Theorem 2.** The coverage probability of the attached UAV-Rx  $u_i^v$  conditioned on the distance  $r_i^v$  and the UAV's flight height  $h_{v_i}$  is given in (36).

*Proof.* Please refer to Appendix C for the proof.

## C. Area Spectral Efficiency

The ASE of UAV and D2D networks can be obtained from the previous results. We denote the PDF of the distance between UAV-Rx and the ground projection of its associated UAV as  $f_{r_{i}^{v}}(r)$ . For example, if we consider that  $r_i^v$  is uniformly distributed in a circular region centered at the projection of UAV  $v_i$  with radius  $R_{\text{max}}$ , then we have  $\begin{array}{c} f_{r_i^v}\left(r\right) = \frac{2r}{R_{\max}^2}, r \geqslant 0. \\ \text{The ASE of UAV networks is given by} \end{array}$ 

$$ASE_{V} = \frac{T - \tau}{T} \left( \sum_{n=1}^{N_{h}} P_{UAV}^{act,n} \lambda_{V,H_{n}} \overline{\mathbb{P}_{V}^{c}} \middle| H_{n} \right) + \sum_{n=N_{h}+1}^{N} P^{0} \lambda_{V,H_{n}} \overline{\mathbb{P}_{V}^{c}} \middle| H_{n} \right) \log_{2} \left( 1 + \gamma_{V}^{th} \right),$$
(37)

where  $N_h$  satisfies that  $H_{N_h} \approx \mathcal{R}_s$ ,  $\overline{\mathbb{P}_V^c} | H_n =$  $\mathbb{E}_r \{ \mathbb{P}_V^c | r, H_n \}, \, \mathbb{P}_V^c | r, H_n \text{ is given in Theorem 2, and } P_{UAV}^{act,n}$ is obtained in (34).

The ASE of D2D networks is given by

$$ASE_D = \lambda_D \overline{\mathbb{P}_D^c} \log_2 \left( 1 + \gamma_D^{th} \right), \tag{38}$$

where  $\overline{\mathbb{P}^c_D} = \mathbb{E}_l \left\{ \mathbb{P}^c_D | l \right\}$  and  $\mathbb{P}^c_D | l$  is given in (35).

Based on our analytical framework, we can maximize the ASE of UAV networks while guaranteeing that the ASE of D2D networks is not below a certain value  $\vartheta$ , as follows

$$\max_{\mathcal{R}_s} ASE_V$$
s.t.  $ASE_D \geqslant \vartheta$ . (39)

where  $ASE_V$  and  $ASE_D$  are given in (37) and (38), respectively,  $\vartheta$  denotes the ASE threshold of D2D networks. It is worth noting that decreasing  $\mathcal{R}_s$  leads to a more aggressive

$$\begin{split} & \mathbb{P}_{V}^{c}|r_{i}^{v},h_{v_{i}} \approx \sum_{m=1}^{M} \left\{ \left( \begin{array}{c} M \\ m \end{array} \right) (-1)^{m+1} \exp \left( -\frac{2\pi^{2}\lambda_{D} \left( \frac{m_{SV\gamma_{V}^{th}P_{D}}}{P_{V}L(v_{i},u_{i}^{v})} \right)^{\frac{2}{\alpha_{GG}}}}{\alpha_{GG} \sin \left( \frac{2\pi}{\alpha_{GG}} \right)} \left( (r_{i}^{v})^{2} + (h_{v_{i}})^{2} \right)^{\frac{\alpha_{AG}}{\alpha_{GG}}} \right) \\ & \cdot \exp \left[ -2\pi \left( \sum_{n=1}^{N_{h}} P_{UAV}^{act,n} \lambda_{V,H_{n}} \int_{0}^{\infty} x\Xi\left(m,x,H_{n},r_{i}^{v},h_{v_{i}}\right) dx + \sum_{n=N_{h}+1}^{N} P^{0}\lambda_{V,H_{n}} \int_{0}^{\infty} x\Xi\left(m,x,H_{n},r_{i}^{v},h_{v_{i}}\right) dx \right) \right] \\ & \cdot \exp \left( -\frac{m\eta_{M}\gamma_{V}^{th}\sigma_{n}^{2}}{P_{V}L\left(v_{i},u_{i}^{v}\right)\left(\left(r_{i}^{v}\right)^{2} + (h_{v_{i}})^{2}\right)^{-\frac{\alpha_{AG}}{2}}} \right) \right\} \\ & \text{where } L\left(r_{i}^{v},h_{v_{i}}\right) = \frac{1}{1+C\exp\left[-B\left(E\arctan\left(\frac{h_{v_{i}}}{r_{i}^{v}}\right) - C\right)\right]} + \eta \left(1 - \frac{1}{1+C\exp\left[-B\left(E\arctan\left(\frac{h_{v_{i}}}{r_{i}^{v}}\right) - C\right)\right]} \right) \\ & \Xi\left(m,x,H_{n},r_{i}^{v},h_{v_{i}}\right) \\ & = 1 - \left[1+\Delta\left(x,H_{n}\right)\frac{m\eta_{M}\gamma_{V}^{th}\left(x^{2} + H_{n}^{2}\right)^{-\frac{\alpha_{AG}}{2}}}{ML\left(v_{i},u_{i}^{v}\right)\left(\left(r_{i}^{v}\right)^{2} + (h_{v_{i}})^{2}\right)^{-\frac{\alpha_{AG}}{2}}} + (1-\Delta\left(x,H_{n}\right))\frac{m\eta_{M}\gamma_{V}^{th}\eta\left(x^{2} + H_{n}^{2}\right)^{-\frac{\alpha_{AG}}{2}}}{ML\left(v_{i},u_{i}^{v}\right)\left(\left(r_{i}^{v}\right)^{2} + (h_{v_{i}})^{2}\right)^{-\frac{\alpha_{AG}}{2}}} \right]^{-M}, \end{aligned}$$

spectrum reuse for UAV communications; however, it also generates more severe co-channel interference, which reduces the D2D communications performance. Therefore, there is a clear trade-off between aggressive spectrum reuse and co-channel interference. Alternatively, based on our model, one can evaluate the entire network performance using the weighted Tchebycheff method [31] and obtain the Paretooptimality criterion for spectrum sharing between UAV and D2D communications. To solve the problem 39, we leverage the one-dimensional numerical search method using the closed-form expressions of ASEs for both the UAV and D2D networks. It is worth noting that the ASE of both the UAV and D2D networks can be approximated by the machine learning approach. However, it involves many input network parameters which makes the data set generation difficult. In addition, when the operation of networks changes, the scalability of the approach that directly approximates the ASE by machine learning is insufficient.

#### V. SIMULATION RESULTS AND DISCUSSION

In this section, we verify our analysis by simulations and evaluate the performance of the D2D and UAV spectrum sharing networks. The simulated network uses the following parameter settings, unless otherwise stated:  $\lambda_D=1\times 10^{-5}/\text{m}^2$ ,  $\lambda_V=1\times 10^{-5}/\text{m}^2$ ,  $P_D=20\text{mW}$ ,  $P_V=20\text{mW}$ , M=1, N=10,  $H_{min}=10\text{m}$ ,  $H_{max}=100\text{m}$ ,  $\alpha_{GG}=4$ ,  $\alpha_{GA}=\alpha_{AG}=2.1$ ,  $P_{fa}^*=0.1$ ,  $\sigma_n^2=-110\text{dBm}$ ,  $\beta_0=0.8$ ,  $\beta_1=0.16$  [14],  $\eta=0.1$ , B=0.136 and C=11.95 [23].

In Fig. 4, we show a 3D network for the coexistence of D2D and UAV communications. D2D-Txs are uniformly distributed on the ground with the density  $\lambda_D = 1 \times 10^{-5}/\text{m}^2$ . D2D-Rxs are located at positions with random directions and distances to its associated D2D-Txs between 20m and 80m. The UAVs

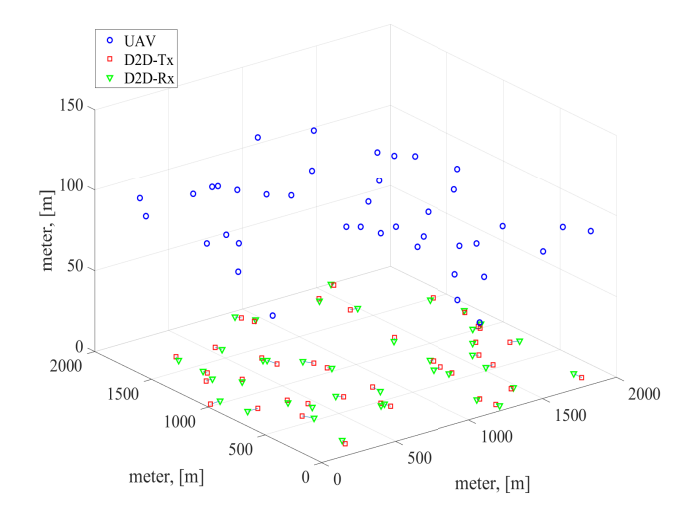


Fig 4: Simulation scenario where D2D-Txs are uniformly distributed on the ground and UAVs are uniformly distributed in the allowable flight space within the height of [10m, 100m].

are uniformly distributed in the aerial 3D space at a height of [10m, 100m]. The density of the projections of UAVs on the ground is  $\lambda_V=1\times 10^{-5}/\text{m}^2$ .

Fig. 5 compares the PDF of the received signal strength at a UAV for the event  $\mathcal{H}^0$ , where the UAV is at a height of 60m and has the spatial spectrum sensing radius of  $\mathcal{R}_s=150$ m. The results are obtained from Monte-Carlo simulations, whereas the red dashed line is obtained by the proposed machine learning-based approximation in Section III-C. We observe that the proposed approximation method accurately depicts the PDF of the received aggregated power generated from ground D2D communications for the event

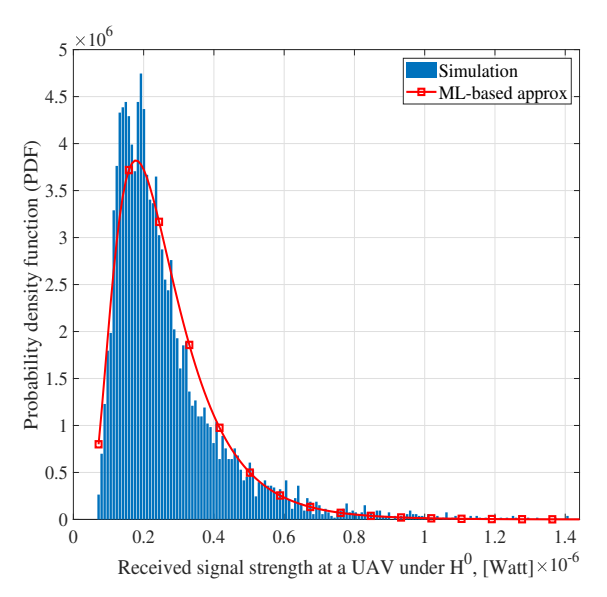


Fig 5: PDF of a the received signal strength at the UAV during spatial spectrum sensing for the false alarm case and the flight height of  $h_v=60$ m,  $\mathcal{R}_s=150$ m.

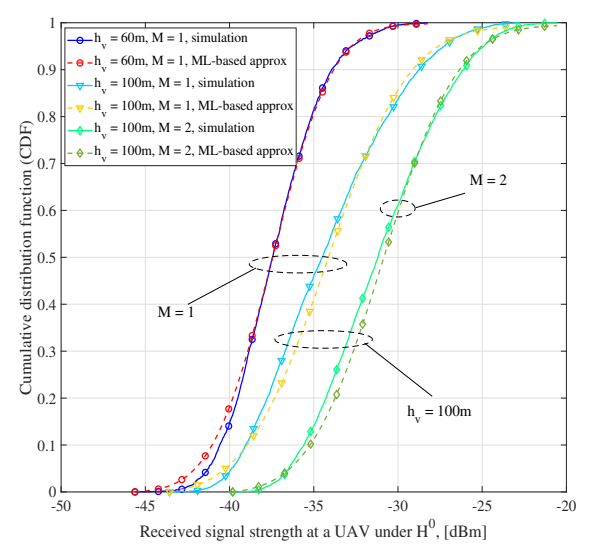


Fig 6: CDF of a UAV's received signal strength during spatial spectrum sensing for the false alarm case, where  $\mathcal{R}_s=150$ m.

 $\mathcal{H}^0$  during spatial spectrum sensing. The complexity of the Monte-Carlo simulations are more time-consuming than the proposed ML-based approach. This is because the ML-based approach needs to collect the data set in the early stage before the training process, whereas the trained distributions can be used permanently. However, for the Monte-Carlo simulations, we need to average multiple independent trials to obtain a stable performance, and, in each trial, the calculation of the network interference at each node is time-consuming.

Fig. 6 shows the cumulative distribution functions (CDFs) of the received signal strength at a UAV for the event  $\mathcal{H}^0$ . We observe that the machine learning-based approximation method well approximates the distribution of the received aggregate power from D2D communications for the event  $\mathcal{H}^0$ . In addition, we observe that when the UAV flight height increases, the received signal strength improves. This is because an increase in UAV height results in a decrease of the radius

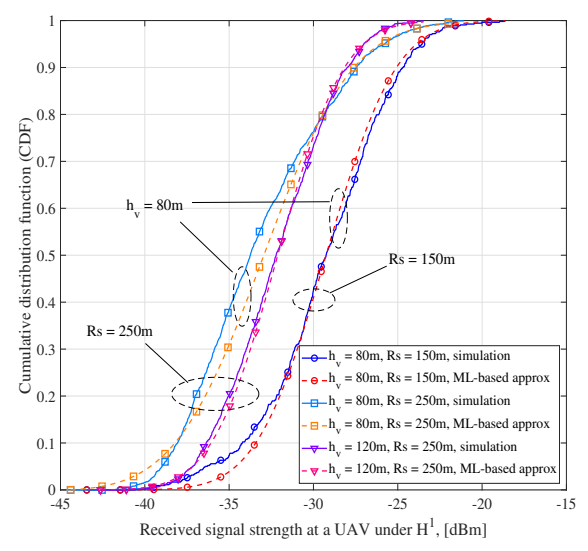


Fig 7: CDF of a UAV's received signal strength during spatial spectrum sensing in missed detection for different UAV flight heights and spatial spectrum sensing radiuses.

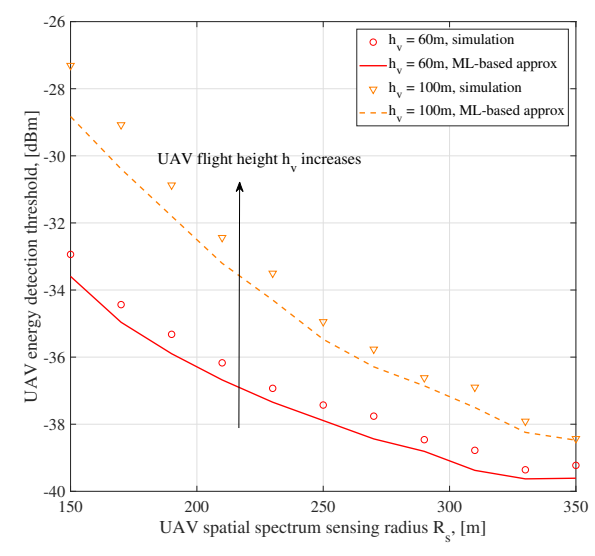


Fig 8: UAV energy detection threshold  $\varepsilon$  with respect to the UAV spatial spectrum sensing radius  $\mathcal{R}_s$ .

of  $\mathcal{A}_{v_i}$  defined in (5) and improves the probability of LOS connections between D2D-Txs and UAV due to the increased elevation angle. Besides, a higher value of small-scale fading parameter M improves the received signal strength.

In Fig. 7, the CDFs of received signal strength at a UAV for the event  $\mathcal{H}^1$  are shown. When  $\mathcal{R}_s$  increases, the received signal strength at a UAV under  $\mathcal{H}^1$  decreases, because of the longer distances between D2D-Txs and the UAV and the higher probability of their NLOS connections in these scenarios. In addition, when a UAV's flight height increases, the received signal strength increases. The reason behind this is similar to that of Fig. 6.

In Fig. 8, we compare the UAV energy detection threshold  $\varepsilon$  with respect to UAV spatial spectrum sensing radius  $\mathcal{R}_s$ . Using the Neyman-Pearson criterion and assuming  $P_{fa}=P_{fa}^*$ , there exists a mapping between  $\mathcal{R}_s$  and  $\varepsilon$ . It can be observed that  $\varepsilon$  decreases with  $\mathcal{R}_s$ . This is because the received

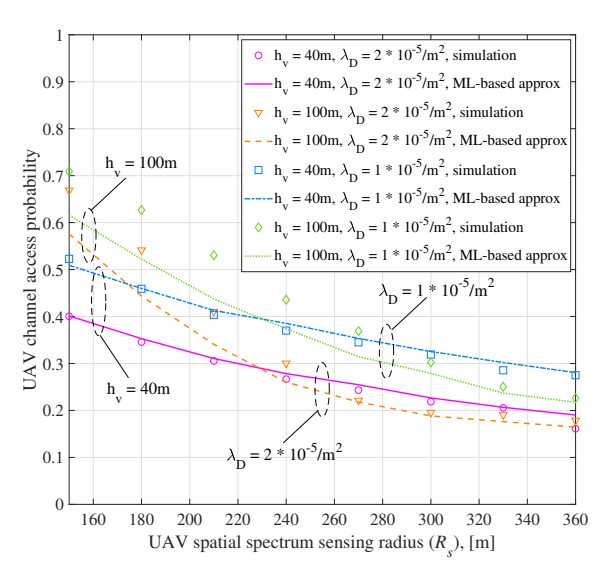


Fig 9: UAV channel access probability with respect to the UAV spatial spectrum sensing radius  $\mathcal{R}_{\circ}$ .

signal strength  $I^0$  under  $\mathcal{H}^0$  decreases as  $\mathcal{R}_s$  increases. To achieve the target  $P_{fa}^*$ , the energy detection threshold needs to be accordingly reduced. In addition, when the UAV's flight height  $h_v$  increases, its energy detection threshold increases, because UAVs at higher heights receive more power from D2D communications under the event  $\mathcal{H}^0$  as shown in Fig. 6. In Fig. 8, we observe that the proposed machine learning-based approximation cannot exactly describe the simulated  $\varepsilon$ . The reason for this is that the distribution of  $I^0$  is not coincidentally the assumed log-normal distribution. However, we train the log-normal distribution parameters to approach the real  $I^0$  distribution.

Fig. 9 plots the UAV channel access probability which is given in (34) over the UAV spatial spectrum sensing radius  $\mathcal{R}_s$ . It can be observed that the UAV channel access probability decreases with  $\mathcal{R}_s$ . This can be explained as follows: under the assumption of  $\beta_0 > \beta_1$ , increasing  $\mathcal{R}_s$  results in a decrease of the UAV energy detection threshold according to Fig. 8. Thus, a UAV has a high probability of transmitting with probability  $\beta_1$ . Therefore, adjusting  $\mathcal{R}_s$  can regulate the density of active UAVs and hence, the interference power due to UAV communications. More specifically, decreasing  $\mathcal{R}_s$  leads to more severe interference generated from UAVs. It can be observed from Fig. 9 that when the density of D2D-Txs becomes large, the UAV channel access probability reduces accordingly due to the incremental received signal strength from D2D-Txs at a UAV during spatial spectrum sensing. We can also find that, when  $\mathcal{R}_s$  is small, increasing the UAV's flight height improves the UAV channel access probability. However, when  $\mathcal{R}_s$  is large, increasing the UAV's height decreases its channel access probability. The rationale behind this is that when  $\mathcal{R}_s$  is small, increasing the height largely increases the UAV's energy detection threshold. The energy detection thresholds for different UAV flight heights is not obvious when  $\mathcal{R}_s$  is large, according to Fig. 8. On the other hand, based on the observation from the simulations, the values of total signal strength received from D2D-Txs are

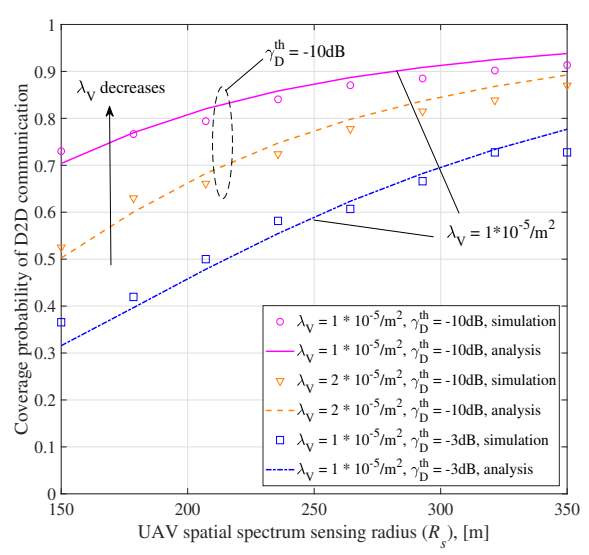


Fig 10: Coverage probability of a typical D2D communication vs. the UAV spatial spectrum sensing radius  $\mathcal{R}_s$ , where  $l_k^d=30m$ .

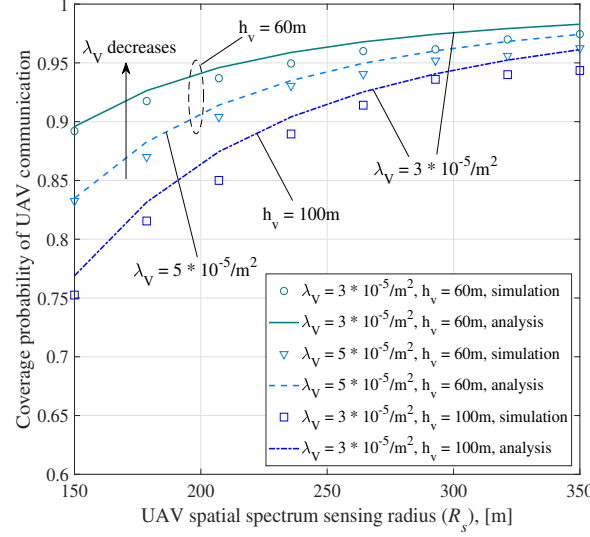


Fig 11: Coverage probability of a typical UAV communications vs. the UAV's spatial spectrum sensing radius  $\mathcal{R}_s$ , where  $r_v=30m$ .

more concentrated around small values for a lower flight height than that for higher heights. Therefore, these can illustrate the behaviour of the crossover point of the UAV channel access probability for different flight height with respect to the UAV's spatial spectrum sensing radius.

In Fig. 10, the coverage probability of D2D communication is presented with respect to the UAV's spatial spectrum sensing radius  $\mathcal{R}_s$ . As can be seen, increasing  $\mathcal{R}_s$  is beneficial to D2D communications. This is so because a larger value of  $\mathcal{R}_s$  makes the UAV more sensitive of the radio environment and reduces its channel access probability, which reduces the interference from UAVs to D2D communications. Besides, reducing the density of UAVs improves the coverage probability of D2D communications. Furthermore, from Fig. 10 we can observe that when  $\mathcal{R}_s$  is small, the SINR threshold of D2D communications  $\gamma_D^{th}$  has a significant impact on the D2D communications coverage probability.

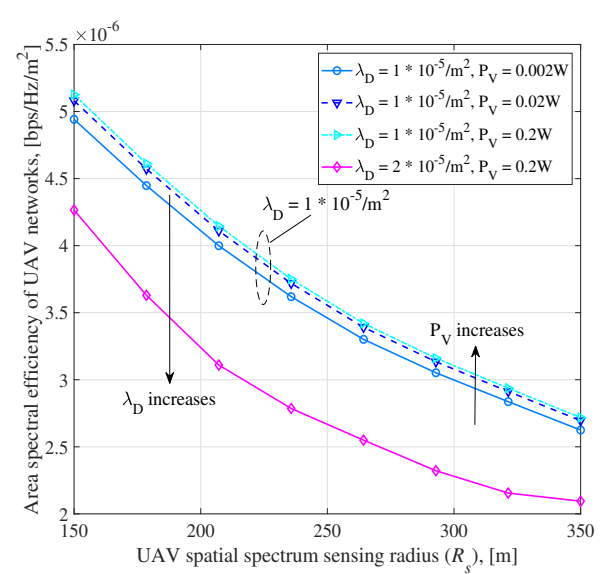


Fig 12: ASE of UAV networks vs. the UAV's spatial spectrum sensing radius  $\mathcal{R}_s$ , where  $r_v=30m,\,P_D=0.2W.$ 

Fig. 11 plots the coverage probability of UAV communication as a function of the UAV's spatial spectrum sensing radius  $\mathcal{R}_s$ . It can be observed that the coverage probability of a typical UAV communication link increases with  $\mathcal{R}_s$  due to the reduced co-channel interference generated from active UAVs. The coverage probability decreases with increasing density of UAVs  $\lambda_V$  and the increasing flight height  $h_V$ . The decrease of  $h_V$  results in the reduction of the serving link distance and thus enhances the desired signal strength at the UAV-Rx, despite the decreasing LOS occurrence probability. Compared with Fig. 9, when  $\mathcal{R}_s$  is small, there is a trade-off between UAV channel access probability and coverage probability. On the other hand, when  $\mathcal{R}_s$  is large, it is advantageous for a UAV that has a lower flight height in terms of both coverage probability and channel access probability.

In Fig. 12, we compare the relate between the ASE of UAV networks  $ASE_V$  and the UAV's spatial spectrum sensing radius  $\mathcal{R}_s$ . The  $ASE_V$  decreases with  $\mathcal{R}_s$  since the reduction of UAV channel access probability dominates the ASE of UAV networks. According to (39), when the ASE of D2D networks is guaranteed not less than a certain value  $\vartheta$ , according to Fig. 10, we can obtain a minimum  $\mathcal{R}_s$  which maximizes  $ASE_V$ . Besides, when increasing the UAV's transmit power  $P_V$ , we observe that the  $ASE_V$  increases. This is because of the improvement of the desired signal strength of UAV communications, while the impact of interference from D2D-Txs gradually diminished. However, increasing  $P_V$  deteriorates the coverage probability of D2D communications and thus the ASE of D2D networks. Therefore, there exists an optimal transmit power for UAVs to maximize the ASE of UAV networks under the constraint of the minimum  $ASE_D$ . Also, when the density of D2D-Txs increases,  $ASE_V$  decreases due to the increased interference from D2D communications.

#### VI. CONCLUSIONS

In this paper, we develop a machine learning-assisted stochastic geometry framework for spectrum sharing between

ground D2D and UAV communications. The D2D-Txs are regarded as the primary users while UAVs opportunistically access the licensed channel by implementing spatial spectrum sensing. We first analyze the spatial false alarm probability and the spatial missed detection probability of a typical UAV. Then, we derive the coverage probability of typical D2D-Rx and typical UAV-Rx, respectively. The ASEs of D2D and UAV networks are also characterized. The results show that a decrease in the spatial spectrum sensing radius of UAVs reduces the coverage probability of UAV communications, but it improves the ASE of UAV networks although the inter-UAV interference increases. The proposed tools allow obtaining the optimal spatial spectrum sensing radius of UAVs to maximize the ASE of UAV networks while guaranteeing the minimum ASE of D2D networks. In addition, the optimal transmit power of UAVs can be obtained to maximize the ASE of UAV networks while guaranteeing the performance of D2D communications.

# APPENDIX B PROOF OF LEMMA 1

Considering that there is at least one D2D-Tx in the  $A_{v_i}$  under the case of  $\mathcal{H}^1$ , we can straightforwardly obtain the test statistics  $\Gamma$  under  $\mathcal{H}^1$  is greater than that under  $\mathcal{H}^0$ , as follows

$$\mathbb{P}\left(\Gamma > \varepsilon | \mathcal{H}^{1}, I^{1}\right) > \mathbb{P}\left(\Gamma > \varepsilon | \mathcal{H}^{0}, I^{0}\right)$$
  

$$\Leftrightarrow (1 - P_{md}) > P_{fa},$$
(40)

where  $\varepsilon$  is the energy detection threshold. In addition, we have

$$P^{0} - P^{1} = (P_{fa} - 1 + P_{md}) \beta_{1} + (1 - P_{fa} - P_{md}) \beta_{0}$$

$$= -[(1 - P_{md}) - P_{fa}] \beta_{1} + [(1 - P_{md}) - P_{fa}] \beta_{0}$$

$$= [(1 - P_{md}) - P_{fa}] (\beta_{0} - \beta_{1}) > 0,$$
(41)

where  $\beta_0 > \beta_1$  in the system model.

Therefore,  $P^0 > P^1$  holds, which completes the proof.

# APPENDIX B PROOF OF THEOREM 1

According to (1), conditioned on the D2D serving distance  $l_k^d = \left\| d_k - u_k^d \right\|$ , the coverage probability of a typical D2D-Rx  $u_k^d$  is given by

$$\mathbb{P}_{D}^{c} \mid l_{k}^{d} \\
= \mathbb{P} \left\{ SINR \left( u_{k}^{d} \right) \geqslant \gamma_{D}^{th} \right\} \\
= \mathbb{P} \left\{ h_{d_{k}u_{k}^{d}} \geqslant \frac{\gamma_{D}^{th} \left( I_{u_{k}^{d}}^{V} + I_{u_{k}^{d}}^{D} + \sigma_{n}^{2} \right)}{P_{D} \left( l_{k}^{d} \right)^{-\alpha_{GG}}} \middle| l_{k}^{d} = \left\| d_{k} - u_{k}^{d} \right\| \right\} \\
= \mathcal{L}_{I_{u_{k}^{d}}^{D}} \left( \frac{\gamma_{D}^{th}}{P_{D} \left( l_{k}^{d} \right)^{-\alpha_{GG}}} \right) \mathcal{L}_{I_{u_{k}^{d}}^{V}} \left( \frac{\gamma_{D}^{th}}{P_{D} \left( l_{k}^{d} \right)^{-\alpha_{GG}}} \right) \\
\cdot \exp \left( -\frac{\gamma_{D}^{th} \sigma_{n}^{2}}{P_{D} \left( l_{k}^{d} \right)^{-\alpha_{GG}}} \right). \tag{42}$$

$$\bigcup_{n=1}^{N_{h}} \mathcal{L}_{I_{u_{k}}^{V,n}}(s) = \mathbb{E} \left\{ \exp \left[ -s \sum_{n=1}^{N_{h}} \sum_{v_{j}^{H_{n}} \in \Phi_{V,H_{n}}^{L}} \frac{P_{NLOS}\left(v_{j}^{H_{n}}, u_{k}^{d}\right) P_{V} \eta g_{v_{j}^{H_{n}} u_{k}^{d}}}{\left\|v_{j}^{H_{n}} - u_{k}^{d}\right\|^{\alpha_{AG}}} + \frac{P_{LOS}\left(v_{j}^{H_{n}}, u_{k}^{d}\right) P_{V} g_{v_{j}^{H_{n}} u_{k}^{d}}}{\left\|v_{j}^{H_{n}} - u_{k}^{d}\right\|^{\alpha_{AG}}} \right] \right\}, \\
\approx \exp \left\{ -\sum_{n=1}^{N_{h}} 2\pi P_{UAV}^{act,n} \lambda_{V,H_{n}} \int_{\sqrt{\mathcal{R}_{s}^{2} - H_{n}^{2}}}^{\infty} x \left[ 1 - (1 + \xi'(x, P_{V}, H_{n}) + \Theta'(x, P_{V}, H_{n}))^{-M} \right] dx \right\}, \\
\text{where } \xi'(x, P_{V}, H_{n}) = \frac{s \eta_{M} P_{V} \left(x^{2} + H_{n}^{2}\right)^{-\frac{\alpha_{AG}}{2}}}{1 + C \exp\left[ -B\left(E \arctan\left(H_{n}/x\right) - C\right)\right]}, \\
\Theta'(x, P_{V}, H_{n}) = \frac{\eta_{M} P_{V} \eta\left(x^{2} + H_{n}^{2}\right)^{-\frac{\alpha_{AG}}{2}}}{M} - \eta \xi'(x, P_{V}), \\$$

More specifically, we have

$$\mathcal{L}_{I_{u_{k}^{D}}}(s)$$

$$= \mathbb{E} \left\{ \exp \left( -s \sum_{d_{j} \in \Phi_{D}, d_{j} \neq d_{k}} P_{D} h_{d_{j} u_{k}^{d}} \left\| d_{j} - u_{k}^{d} \right\|^{-\alpha_{GG}} \right) \right\}$$

$$= \exp \left( -\frac{2\pi^{2} \lambda_{D} (sP_{D})^{\frac{2}{\alpha_{GG}}}}{\alpha_{GG} \sin \left( \frac{2\pi}{\alpha_{GG}} \right)} \right).$$
(43)

We define an integer  $N_h$  satisfying  $\Phi_{V,H_n}$  will  $H_{N_h} \approx \mathcal{R}_s$ . The interference power generated from UAVs is obtained by a summation of each sub-region as follows

$$I_{u_k^d}^V = \sum_{n=1}^{N_h} I_{u_k^d}^{V,n} + \sum_{n=N_h+1}^{N} I_{u_k^d}^{V,n}, \tag{44}$$

The Laplace transform of the interference power from UAVs at a typical D2D-Rx  $u_k^d$  is

$$\mathcal{L}_{I_{u_{k}^{l}}^{V}}(s) = \bigcup_{n=1}^{N_{h}} \mathcal{L}_{I_{u_{k}^{l}}^{V,n}}(s) \bigcup_{n=N_{h}+1}^{\infty} \mathcal{L}_{I_{u_{k}^{l}}^{V,n}}(s). \tag{45}$$

In addition, we have (46). In (46), we approximately consider the interference at the typical D2D-Tx instead of at the typical D2D-Rx for analytical tractability.

When  $n > N_h$ , the flight heights of UAVs exceed the spatial spectrum sensing radius  $\mathcal{R}_s$ . Thus, based on the anlytical framework, UAVs will transmit with probability  $P^0$ .

Therefore, the Laplace transform of  $\sum_{n=N_h+1}^{N} I_{u_k^d}^{V,n}$  is obtained by substituting  $P^0$  for  $P_{UAV}^{act,n}$  in (46) and letting the lower limit of integral to be

limit of integral to be zero.

Combining (43), (45) into (42), we obtain the coverage probability of a typical D2D-Rx as in (35), which completes the proof.

# APPENDIX C PROOF OF THEOREM 2

The serving distance of UAV  $u_i^v$  is denoted by  $l_i^v$ , where  ${l_i^{v}}^2 = {r_i^{v}}^2 + {h_{v_i}}^2$ .

According to (3), conditioned on  $r_i^v$  and  $h_{v_i}$ , the coverage probability of UAV-Rx  $u_i^v$  is

$$\mathbb{P}_{V}^{v} | r_{i}^{v}, h_{v_{i}} \\
= \mathbb{P} \left\{ SINR \left( u_{i}^{v} \right) \geqslant \gamma_{V}^{th} | r_{i}^{v}, h_{v_{i}} \right\} \\
= \mathbb{P} \left\{ SINR \left( u_{i}^{v} \right) \geqslant \gamma_{V}^{th} | r_{u_{i}^{v}}^{v}, h_{v_{i}} \right\} \\
= \mathbb{P} \left\{ g_{v_{i}u_{i}^{v}} \geqslant \frac{\gamma_{V}^{th} I_{u_{i}^{v}}^{agg}}{P_{V}L \left( v_{i}, u_{i}^{v} \right) \left( l_{i}^{v} \right)^{-\alpha_{AG}}} \middle| r_{i}^{v}, h_{v_{i}} \right\} \\
\stackrel{(a)}{\approx} 1 - \mathbb{E} \left\{ \left[ 1 - \exp \left( -\frac{\eta_{M} \gamma_{V}^{th} I_{u_{i}^{v}}^{agg}}{P_{V}L \left( v_{i}, u_{i}^{v} \right) \left( l_{i}^{v} \right)^{-\alpha_{AG}}} \right) \right]^{M} \right\} \\
\stackrel{(b)}{=} 1 - \sum_{n=0}^{M} \binom{M}{n} \mathbb{E} \left\{ e^{-\frac{\eta_{M} \gamma_{V}^{th} I_{u_{i}^{v}}^{agg}}{P_{V}L \left( v_{i}, u_{i}^{v} \right) \left( l_{i}^{v} \right)^{-\alpha_{AG}}} \right\}^{n} \\
= \sum_{n=1}^{M} \binom{M}{n} \left( -1 \right)^{n+1} \mathbb{E} \left\{ e^{-\frac{\eta_{M} \gamma_{V}^{th} I_{u_{i}^{v}}^{th}}{P_{V}L \left( v_{i}, u_{i}^{v} \right) \left( l_{i}^{v} \right)^{-\alpha_{AG}}} I_{u_{i}^{v}}^{agg}} \right\} \\
= \sum_{n=1}^{M} \binom{M}{n} \left( -1 \right)^{n+1} \mathcal{L}_{I_{u_{i}^{v}}^{u}} \left( s \right) \mathcal{L}_{I_{u_{i}^{v}}^{v}} \left( s \right) e^{-s\sigma_{n}^{2}},$$

where  $I_{u_i^v}^{agg} = I_{u_i^v}^V + I_{u_i^v}^D + \sigma_n^2$  is the aggregated interference and noise power at  $u_i^v$ ,  $s = \frac{n\eta_M\gamma_V^{th}}{P_VL(v_i,u_i^v)(l_i^v)^{-\alpha_{AG}}}$  and  $L\left(v_i,u_i^v\right) = P_{LOS}\left(v_i,u_i^v\right) + \eta P_{NLOS}\left(v_i,u_i^v\right)$  is given in (36), (a) is obtained by the approximation of normalized gamma distribution of  $g_{v_i u_i^v}$  [32], (b) is obtained from Binomial theorem. Specifically, we have

$$\mathcal{L}_{I_{u_i^v}^D}(s) \\
= \mathbb{E} \left\{ \exp \left( -s \sum_{d_j \in \Phi_D} P_D h_{d_j u_k^d} \| d_j - u_i^v \|^{-\alpha_{GG}} \right) \right\} \\
\approx \exp \left( -\frac{2\pi^2 \lambda_D (sP_D)^{\frac{2}{\alpha_{GG}}}}{\alpha_{GG} \sin \left( \frac{2\pi}{\alpha_{GG}} \right)} \right). \tag{48}$$

Similar to (44) and (45), the Laplace transform of the interference power from UAVs is

$$\mathcal{L}_{I_{u_{i}^{v}}^{v}}(s) = \bigcup_{n=1}^{N_{h}} \mathcal{L}_{I_{u_{i}^{v}}^{v,n}}(s) \bigcup_{n=N_{h}+1}^{N} \mathcal{L}_{I_{u_{i}^{v}}^{v,n}}(s).$$
 (49)

The results of (49) can be obtained with the similar methods to (46).

Finally, combining (48) and (49) into (47), we can obtain the desired results.

#### REFERENCES

- [1] Y. Zeng, R. Zhang, and T. J. Lim, "Wireless communications with unmanned aerial vehicles: opportunities and challenges," *IEEE Communications Magazine*, vol. 54, no. 5, pp. 36–42, May 2016.
- [2] B. Shang, L. Liu, J. Ma, and P. Fan, "Unmanned aerial vehicle meets vehicle-to-everything in secure communications," *IEEE Communica*tions Magazine, vol. 57, no. 10, pp. 98–103, October 2019.
- [3] J. Kakar and V. Marojevic, "Waveform and spectrum management for unmanned aerial systems beyond 2025," in 2017 IEEE 28th Annual International Symposium on Personal, Indoor, and Mobile Radio Communications (PIMRC), Oct 2017, pp. 1–5.
- [4] B. Shang, L. Zhao, K. Chen, and X. Chu, "Wireless-powered device-to-device-assisted offloading in cellular networks," *IEEE Transactions on Green Communications and Networking*, vol. 2, no. 4, pp. 1012–1026, Dec 2018.
- [5] S. Wu, R. Atat, N. Mastronarde, and L. Liu, "Improving the coverage and spectral efficiency of millimeter-wave cellular networks using device-to-device relays," *IEEE Transactions on Communications*, vol. 66, no. 5, pp. 2251–2265, 2018.
- [6] B. Shang, L. Zhao, K. C. Chen, and X. Chu, "An economic aspect of device-to-device assisted offloading in cellular networks," *IEEE Transactions on Wireless Communications*, vol. 17, no. 4, pp. 2289–2304, April 2018.
- [7] H. Chen, L. Liu, J. D. Matyjas, and M. J. Medley, "Optimal resource allocation for sensing-based spectrum sharing d2d networks," *Computers & Electrical Engineering*, vol. 44, pp. 107–121, 2015.
- [8] B. Shang, L. Zhao, and K. C. Chen, "Enabling device-to-device communications in LTE-unlicensed spectrum," in 2017 IEEE International Conference on Communications (ICC), May 2017, pp. 1–6.
- [9] X. Lin, J. G. Andrews, and A. Ghosh, "Spectrum sharing for device-to-device communication in cellular networks," *IEEE Transactions on Wireless Communications*, vol. 13, no. 12, pp. 6727–6740, Dec 2014.
- [10] Y. R. Ramadan, H. Minn, and Y. Dai, "A new paradigm for spectrum sharing between cellular wireless communications and radio astronomy systems," *IEEE Transactions on Communications*, vol. 65, no. 9, pp. 3985–3999, Sep. 2017.
- [11] Z. Chen and M. Kountouris, "Decentralized opportunistic access for D2D underlaid cellular networks," *IEEE Transactions on Communica*tions, vol. 66, no. 10, pp. 4842–4853, Oct 2018.
- [12] H. Chen, L. Liu, T. Novlan, J. D. Matyjas, B. L. Ng, and J. Zhang, "Spatial spectrum sensing-based device-to-device cellular networks," *IEEE Trans. Wireless Commun.*, vol. 15, no. 11, pp. 7299–7313, Nov 2016.
- [13] R. Atat, L. Liu, H. Chen, J. Wu, H. Li, and Y. Yi, "Enabling cyber-physical communication in 5G cellular networks: Challenges, spatial spectrum sensing, and cyber-security," *IET Cyber-Physical Systems: Theory Applications*, vol. 2, no. 1, pp. 49–54, 2017.
- [14] H. Chen, L. Liu, H. S. Dhillon, and Y. Yi, "Qos-aware d2d cellular networks with spatial spectrum sensing: A stochastic geometry view," *IEEE Transactions on Communications*, vol. 67, no. 5, pp. 3651–3664, May 2019.
- [15] B. Shang, L. Liu, H. Chen, J. Zhang, S. Pudlewski, E. S. Bentley, and J. Ashdown, "Spatial Spectrum Sensing-Based D2D Communications in User-Centric Deployed HetNets," in 2019 IEEE Global Communications Conference (GLOBECOM), Dec 2019, pp. 1–6.
- [16] C. Zhang and W. Zhang, "Spectrum sharing for drone networks," *IEEE Journal on Selected Areas in Communications*, vol. 35, no. 1, pp. 136–144, Jan 2017.
- [17] H. Wang, J. Wang, G. Ding, J. Chen, Y. Li, and Z. Han, "Spectrum sharing planning for full-duplex UAV relaying systems with underlaid D2D communications," *IEEE Journal on Selected Areas in Communications*, vol. 36, no. 9, pp. 1986–1999, Sep. 2018.
- [18] M. Mozaffari, W. Saad, M. Bennis, and M. Debbah, "Unmanned aerial vehicle with underlaid device-to-device communications: Performance and tradeoffs," *IEEE Transactions on Wireless Communications*, vol. 15, no. 6, pp. 3949–3963, June 2016.
- [19] M. M. Selim, M. Rihan, Y. Yang, L. Huang, Z. Quan, and J. Ma, "On the outage probability and power control of D2D underlaying NOMA UAV-assisted networks," *IEEE Access*, vol. 7, pp. 16525–16536, 2019.

- [20] M. Rihan, M. M. Selim, C. Xu, and L. Huang, "D2D communication underlaying UAV on multiple bands in disaster area: Stochastic geometry analysis," *IEEE Access*, vol. 7, pp. 156 646–156 658, 2019.
- [21] M. Bacha, Y. Wu, and B. Clerckx, "Downlink and uplink decoupling in two-tier heterogeneous networks with multi-antenna base stations," *IEEE Transactions on Wireless Communications*, vol. 16, no. 5, pp. 2760–2775, May 2017.
- [22] A. Al-Hourani, S. Kandeepan, and A. Jamalipour, "Modeling air-to-ground path loss for low altitude platforms in urban environments," in 2014 IEEE Global Communications Conference, Dec 2014, pp. 2898– 2904.
- [23] A. Al-Hourani, S. Kandeepan, and S. Lardner, "Optimal LAP altitude for maximum coverage," *IEEE Wireless Communications Letters*, vol. 3, no. 6, pp. 569–572, Dec 2014.
- [24] W. Khawaja, I. Guvenc, and D. Matolak, "UWB channel sounding and modeling for UAV air-to-ground propagation channels," in 2016 IEEE Global Communications Conference (GLOBECOM), Dec 2016, pp. 1–7.
- [25] E. Yanmaz, R. Kuschnig, and C. Bettstetter, "Achieving air-ground communications in 802.11 networks with three-dimensional aerial mobility," in 2013 Proceedings IEEE INFOCOM, April 2013, pp. 120–124.
- [26] Y. Liang, Y. Zeng, E. C. Y. Peh, and A. T. Hoang, "Sensing-throughput tradeoff for cognitive radio networks," *IEEE Transactions on Wireless Communications*, vol. 7, no. 4, pp. 1326–1337, April 2008.
- [27] X. Wu and Z. Ma, "Modeling and performance analysis of cellular and device-to-device heterogeneous networks," in 2017 IEEE Globecom Workshops (GC Wkshps), Dec 2017, pp. 1–6.
- [28] M. Haenggi and R. K. Ganti, "Interference in large wireless networks," Foundations and Trends® in Networking, vol. 3, no. 2, pp. 127–248, 2009.
- [29] Z. Chen, C.-X. Wang, X. Hong, J. S. Thompson, S. A. Vorobyov, X. Ge, H. Xiao, and F. Zhao, "Aggregate interference modeling in cognitive radio networks with power and contention control," *IEEE Transactions* on Communications, vol. 60, no. 2, pp. 456–468, 2012.
- [30] B. Shang and L. Liu, "Machine learning meets point process: Spatial spectrum sensing in user-centric networks," *IEEE Wireless Communica*tions Letters, vol. 9, no. 1, pp. 34–37, Jan 2020.
- [31] H. Qu, R. Tang, J. Zhao, and Z. Cao, "Performance tradeoff between user fairness and energy conservation in downlink NOMA systems," in 2018 IEEE International Conference on Communications Workshops (ICC Workshops), May 2018, pp. 1–6.
- [32] H. Alzer, "On some inequalities for the incomplete gamma function," Mathematics of Computation of the American Mathematical Society, vol. 66, no. 218, pp. 771–778, 1997.